

Balanced Token Pruning: Accelerating Vision Language Models Beyond Local Optimization

Kaiyuan Li^{1*}, Xiaoyue Chen^{1*}, Chen Gao², Yong Li², Xinlei Chen¹

¹Tsinghua Shenzhen International Graduate School

²Tsinghua University

{likaiyua23, chenxiao24}@mails.tsinghua.edu.cn

{chgao96, liyong07}@tsinghua.edu.cn, chen.xinlei@sz.tsinghua.edu.cn

Abstract

Large Vision-Language Models (LVLMs) have shown impressive performance across multi-modal tasks by encoding images into thousands of tokens. However, the large number of image tokens results in significant computational overhead, and the use of dynamic high-resolution inputs further increases this burden. Previous approaches have attempted to reduce the number of image tokens through token pruning, typically by selecting tokens based on attention scores or image token diversity. Through empirical studies, we observe that existing methods often overlook the joint impact of pruning on both the current layer’s output (local) and the outputs of subsequent layers (global), leading to suboptimal pruning decisions. To address this challenge, we propose Balanced Token Pruning (BTP), a plug-and-play method for pruning vision tokens. Specifically, our method utilizes a small calibration set to divide the pruning process into multiple stages. In the early stages, our method emphasizes the impact of pruning on subsequent layers, whereas in the deeper stages, the focus shifts toward preserving the consistency of local outputs. Extensive experiments across various LVLMs demonstrate the broad effectiveness of our approach on multiple benchmarks. Our method achieves a 78% compression rate while preserving 96.7% of the original models’ performance on average.

1 Introduction

Recent advances in Large Vision-Language Models (LVLMs) [6, 11, 20, 22, 32] have substantially improved visual understanding. These models typically employ a visual encoder to convert images into discrete tokens, which are then processed jointly with textual tokens by a large language model backbone. The incorporation of visual information significantly increases the total number of input tokens [2, 21], a problem further amplified when handling high-resolution images. In scenarios with constrained computational resources and limited memory capacity, the large volume of visual tokens leads to considerable increases in inference latency and memory usage, thereby limiting the practical applicability of LVLMs in resource-limited environments.

Prior studies have demonstrated that visual tokens often exhibit significant redundancy [5, 19]. Consequently, visual token pruning has been proposed as an effective strategy to reduce input redundancy and enhance computational efficiency [34, 29, 12, 38, 35]. Visual token pruning faces two fundamental challenges: identifying the most important visual tokens and determining the appropriate layers for pruning. Existing token pruning strategies can be broadly classified into two categories: attention-based methods that leverage text-image interactions [5, 33], and diversity-based methods that exploit the heterogeneity of visual representations [1]. However, the impact of

* Equal contribution.

their distinct optimization objectives on overall model performance remains underexplored, and a systematic comparison between them is largely absent. Moreover, when it comes to pruning layer selection, existing methods rely heavily on validation performance and manually defined settings, lacking principled guidance based on the model’s intrinsic properties.

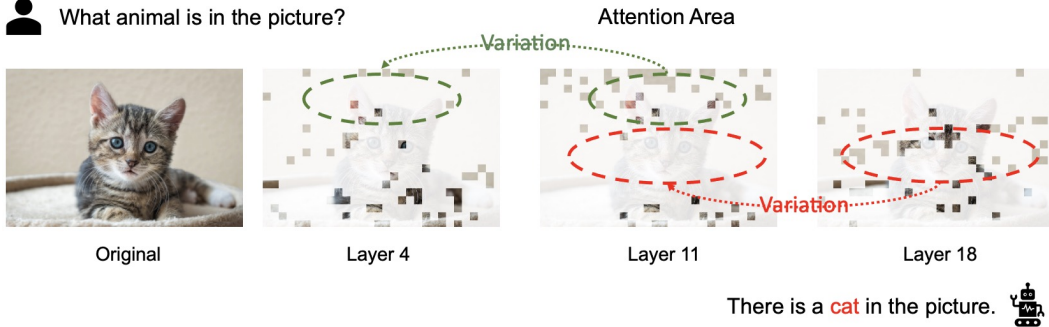


Figure 1: Layer-wise visualization of attention in LVLMs.

To address these problems, we first explore the nature of image token pruning from an intuitive perspective: its impact on the **current layer’s (local)** output and its influence on the outputs of **subsequent pruning layers (global)**. We begin by visualizing the spatial distribution of image tokens that receive higher attention from text tokens across different layers. As shown in Figure 1, we observe that the image tokens attended by text tokens vary across different layers. This indicates that pruning solely based on the current layer tends to overlook its impact on subsequent layers. Then we further compare the similarity between the hidden state of the last word in the input prompt under two pruning methods and that of the original model. It can be found in Figure 2 that attention-based methods preserve output similarity well at early pruning layers, but the error accumulates in deeper layers. In contrast, diversity-based methods do not maintain output similarity at the initial layers, but achieve better consistency in later pruning stages. This implies that attention-based pruning methods focus solely on optimizing the current pruning layer while ignoring their impact on subsequent layers, whereas diversity-based methods overlook the preservation of output quality at the current layer.

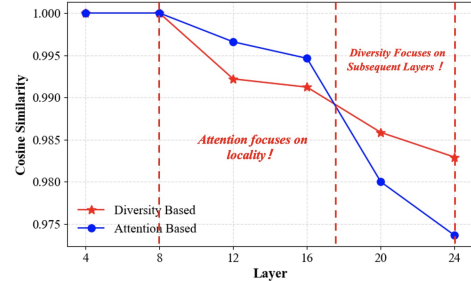


Figure 2: Impact of different pruning strategies on layer-wise representations.

Motivated by the above observation, we aim to tackle a fundamental challenge: *how to prune with joint consideration of the current and subsequent layers to achieve global optimality*. To address this challenge, we propose **Balanced Token Pruning (BTP)**, a visual token pruning method that balances local objectives (current layer) with global objectives (subsequent layers). We begin by analyzing and formulating a local-global objective for image token pruning. Based on this objective, BTP first partitions the pruning process into multiple stages using a small calibration set [27, 14], leveraging the way LVLMs process images, as illustrated in Figure 4. In early stages, where more image tokens are retained, BTP emphasizes a diversity-based objective to preserve the quality of downstream representations. In later stages, where fewer tokens are retained, it prioritizes an attention-based objective to maintain the consistency of local outputs. With this design, we preserve token diversity in the early layers while focusing on task-relevant tokens in the later layers.

Extensive experiments demonstrate the effectiveness of our proposed BTP method. We evaluate BTP across models of varying sizes and architectures, consistently achieving superior performance under higher compression ratios. Notably, our approach retains only 22% of the original image tokens on average while preserving 98% of the model’s original performance. Furthermore, end-to-end efficiency evaluations confirm that BTP significantly reduces both inference latency and memory usage in practice.

2 Related work

2.1 Large Vision-Language Models

Recent progress in large vision language models (LVLMs) has been substantially accelerated by the open-sourcing of foundation models like LLaMA [30] and Vicuna [40]. Representative models, including LLaVA [20, 21, 22], Qwen-VL [2, 32], and InternVL [6, 11] leverage vision encoders [26, 18, 7] to encode images into visual tokens, which are then integrated into the language model for unified multimodal representation and understanding. For example, LLaVA-1.5 encodes image into 576 visual tokens using a single-scale encoder. As these models increasingly support high-resolution visual inputs [2, 21], the number of visual tokens grows. Using a multi-resolution encoding strategy, LLaVA-NeXT can generate up to 2,880 tokens per image.

2.2 Visual Token Pruning

Early efforts to reduce visual token redundancy primarily focus on attention-based pruning [4, 13, 39]. For example, FastV [5] prunes visual tokens with low attention scores after the filtering layer, with subsequent layers processing only the remaining token. Another approach, VTW [19], adopts a complete token elimination strategy, removing all visual tokens after a specified layer. PyramidDrop [33] introduces a more sophisticated approach, performing stage-wise pruning throughout the transformer, ranking visual tokens by their attention scores to the instruction token at each stage and progressively discarding the least informative ones. Compared to attention-based methods, diversity-based methods prioritize retaining a richer variety of semantic information. For instance, DivPrune [1] formulate token pruning as a Max-Min Diversity Problem [25, 28]. Additionally, some methods fuse remaining tokens into retained tokens through token fusion such as LLaVA-PruMerge [29] and VisionZip [34]. Different from prior methods, our method jointly considers the impact of pruning on both the current layer and subsequent layers.

3 Preliminary

3.1 Visual token processing

In the prefilling stage, images and texts are first encoded into embedding vectors (tokens), which are then processed by LVLM. We denote the input token sequence as \mathbf{X} which consists of the system prompt \mathbf{X}_S , the image tokens \mathbf{X}_I and text tokens \mathbf{X}_T , $\mathbf{X} = (\mathbf{X}_S, \mathbf{X}_I, \mathbf{X}_T)$. \mathbf{X} is then fed into the LLM backbone composed of N decoder layers. For the l -th decoder layer, we denote the input as $\mathbf{X}^{(l)}$ and the layer output $\mathbf{X}^{(l+1)}$ is:

$$\mathbf{X}^{(l+1)} = \mathbf{X}^{(l)} + \text{Atten}^{(l)}(\text{LN}(\mathbf{X}^{(l)})) + \text{MLP}^{(l)}(\text{LN}(\text{attn}_{\text{output}}^{(l)} + \mathbf{X}^{(l)})), \quad (1)$$

where $\text{Atten}^{(l)}$ is the attention block, LN is the layer normalization and $\text{MLP}^{(l)}$ is the projector layer. It can be observed that the outputs of the attention block and the MLP block are closely tied to the attention mechanism [31]. Formally, the attention mechanism can be represent as:

$$\text{attn}_{\text{output}}^l = \text{Softmax}\left(\frac{Q_l(K_l)^T + M}{\sqrt{D_k}}\right)V_l, \quad (2)$$

where Q_l , K_l , V_l are calculated by Query projector, Key projector and Value projector. D_k is hidden state dimension. M is the casual mask which imposes a constraint such that each token is permitted to incorporate information only from tokens at earlier positions. K_l , V_l are stored in the KV cache for further decoding stage.

3.2 Visual token pruning formulations

Prior works on image token pruning can be broadly categorized into attention-based methods [5, 33] and diversity-based methods [1]. Attention based methods utilize text-image attention score to select important image tokens at specific layers. For input sample with m text tokens, we can denote the importance score S_{img} of image tokens at l -th layer as:

$$S_{\text{img}}^{(l)} = \frac{1}{m} \sum_{i=1}^m \text{Atten}^{(l)}(\mathbf{X}_I, \mathbf{X}_T^{(i)}). \quad (3)$$

After obtaining the importance scores of the image tokens, these methods select a pruned image token set $\mathbb{P}_{atten} \subset \mathbf{X}_I$ with the highest scores. In contrast to attention score-based methods, diversity-based approaches focus on maximizing the diversity among selected image tokens. These methods are typically based either on the spatial diversity of the selected image token set or on the semantic diversity of the selected images. Formally, given a diversity metric $\mathcal{F} \in \{\mathcal{F}_{spa}, \mathcal{F}_{sem}\}$, our goal is to identify a pruned set of image tokens $\mathbb{P}_{div} \subset \mathbf{X}_I$ that maximizes the objective function \mathcal{L}_{div} :

$$\mathcal{L}_{div} = \max \mathcal{F}(\mathbb{P}_{div}). \quad (4)$$

4 Methodology

4.1 Limitations of existing methods

Attention-based methods pursue local optima We analyze the impact of pruning image tokens on the subsequent text and response tokens. From Equations 1 and 2, we can see that pruning image tokens at l -th layer mainly affects the layer output $\mathbf{X}^{(l+1)}$ by changing the attention output, which is a weighted sum of the value vectors V_l . If the norms of the V_l are similar, selecting image tokens with high importance scores defined in 3 effectively reduces the difference between the layer output before and after pruning. We provide supporting evidence for this assumption in the Appendix A.1. Formally, given original l -th layer output $\mathbf{X}_{origin}^{(l+1)}$ and pruned l -th layer output $\mathbf{X}_{pruned}^{(l+1)}$, distance metric function $D(\cdot, \cdot)$, we can define the objective function \mathcal{L}_{atten} of attention-based methods [5, 33] as:

$$\mathcal{L}_{atten} = \min_{\mathbb{P}} D(\mathbf{X}_{origin}^{(l+1)}, \mathbf{X}_{pruned}^{(l+1)}). \quad (5)$$

However, attention-based methods locally optimize the output error at individual layers. For instance, if pruning is conducted at the l -th layer and $(l+k)$ -th layers, with \mathbb{P}_l and \mathbb{P}_{l+k} denoting the respective optimal sets of selected image tokens. As shown in Figure 1, $\mathbb{P}_{l+k} \not\subset \mathbb{P}_l$. So, attention-based selection results in a **globally suboptimal** pruning strategy.

Diversity-based methods ignore local constraints The diversity-based approach [1] aims to maximize the diversity of the selected tokens, thereby partially mitigating the issues encountered by attention-based methods as we can see in Figure 1. Because diversity-based methods tend to select tokens with maximally different semantic information. However it can be observed in Figure 2 that diversity-based approaches are ineffective in maintaining local output consistency, which can lead to a failure in preserving **local output consistency** during deep-layer pruning, resulting in degraded performance.

Layer selection for pruning Current approaches typically rely on manually predefined pruning layers or utilize a small validation set to select pruning layers based on the observed performance. However, these methods require extensive trial-and-error and dataset-specific calibration. As described in Section 3.1, due to the presence of the causal mask M , the encoding of an image token in the LLM backbone is independent of the input question. Therefore, we aim to determine the pruning layers from the perspective of image token encoding.

4.2 Balanced token pruning with joint local and global objectives

Local-global objective Based on the above analysis, we argue that an effective token pruning strategy should achieve local optimization by preserving the current layer’s output, while also considering the global impact of pruning on subsequent layers. Firstly, we formulate a **global objective** function. Suppose token pruning is performed at layers $l_1 < l_2 < l_3$. For each pruned layer $l \in \{l_1, l_2, l_3\}$, we aim to select a subset of tokens \mathbb{P}_l such that the difference between the pruned outputs X_{pruned}^{l+1} and original outputs X_{origin}^{l+1} is minimized. To quantify hidden vectors’ difference, we use a unified distance function $D(\cdot, \cdot)$ to measure the discrepancy between the outputs before and after pruning. Then our objective is to minimize the total output discrepancy across all pruned layers:

$$\mathcal{L}_{global} = \sum_{i=1}^{|I|} D(X_{origin}^{l+1}, X_{\mathbb{P}_{l_i}}^{l+1}). \quad (6)$$

According to Equation 5, we can get optimal pruned token set \mathbb{P}_l^* based on attention. However, since the attention distribution varies across input samples and $P_{l_3} \subseteq P_{l_2} \subseteq P_{l_1}$, it is difficult to

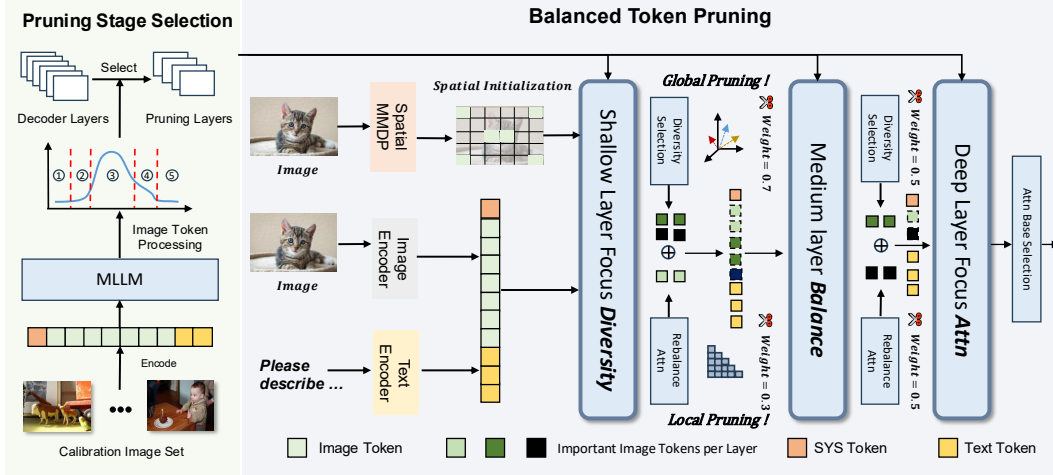


Figure 3: Overview of BTP: We first use a calibration set to determine the pruning layers. In the early layers, we emphasize diversity-based pruning to preserve the output of subsequent layers. In the deeper layers, attention-based pruning is prioritized to maintain the output of the pruning layers. Due to the pruning strategy, we achieve an overall optimal pruning balance.

predict which tokens will be important for deeper layers (e.g., l_2, l_3) when pruning at layer l_1 . To address this issue, we propose to optimize a **local-global objective** to approximate the optimal token set P_l^* . Building upon the local attention-based selection objective, we introduce a diversity term to approximate the token preferences of later layers. Assume a weight coefficient $\lambda \in (0, 1)$, we measure diversity by computing the sum of distance $F_{dis}(\cdot)$ among elements within a set:

$$\mathcal{L}_{local-global} = - \sum_{i=1}^{|I|} (\lambda_i \sum_{j \in P_i} \text{Atten}^{(i)}(\mathbf{X}_I^{(j)}, \mathbf{X}_T) + (1 - \lambda_i) F_{dis}(P_i)). \quad (7)$$

The first term of Equation 7 ensures that the output of the pruned layer remains close to the original, while the second term encourages the selected tokens at previous layer l_1 to also include those important for deeper layers such as l_2 and l_3 .

Balanced token pruning (BTP) Building upon the proposed local-global objective, we introduce our method. As shown in Figure 3, our approach divides token pruning into multiple stages denoted as $\mathcal{S} = \{s_1, \dots, s_n\}$. Under a predefined pruning ratio α , each stage retains a fixed fraction of image tokens from the previous stage. Since early pruning stages retain more tokens and influence the pruning decisions of later stages, their objectives need to emphasize token diversity. In contrast, deeper stages preserve fewer tokens and have less impact on subsequent stages. Therefore, we set the hyperparameter λ_i to gradually increase across stages.

Attention optimization: We optimize the attention objective by selecting the top- k image tokens with the highest importance scores defined in Equation 3. To efficiently computing the importance scores, we only use the last token of the input prompt as \mathbf{X}_T , which reduces the computational complexity to $\mathcal{O}(n)$. We observe that the attention scores are influenced by positional encoding, which leads to a tendency to favor tokens located toward the end of the sequence. We apply a re-balancing operation to alleviate the influence of positional encoding. Assume that at l -th layer, we aim to prune the image tokens by selecting k indices I_k out of N candidates based on the attention scores A_l . Instead of directly selecting the top- k tokens, we first over-select the top- k' tokens indices $I_{k'}$, where $k' > k$. To mitigate positional bias, we rebalance the selection by first retaining tokens from earlier positions, followed by selecting additional tokens from later positions:

$$I_{pre} = I_{k'}[I_{k'} < \frac{N}{2}], \quad (8)$$

$$I_{post} = I_{k'}[I_{k'} \geq \frac{N}{2}][:k - |I_{pre}|], \quad (9)$$

$$I_k = \text{Concat}(I_{pre}, I_{post}). \quad (10)$$

Through the rebalancing operation, we are able to preserve the attention objective while selecting more informative tokens.

Diversity optimization: For optimizing the second objective related to diversity, we follow the formulation used in DivPrune by modeling it as a Max-Min Diversity Problem (MMDP). However, solving the MMDP objective requires $\mathcal{O}(n^2)$ computational complexity and cannot be efficiently accelerated by GPUs, resulting in significant computational latency. This issue becomes more pronounced in high-resolution multimodal models with a larger number of image tokens. To address this challenge, we propose an initialization strategy based on spatial position information. We observe that image patches with large spatial distances tend to exhibit greater semantic differences, while spatially adjacent patches are often semantically similar. Based on this intuition, we initialize the set of selected image tokens by solving an MMDP problem over their spatial positions. Formally, given N image tokens \mathbf{X}_I , which are originally obtained by flattening a 2D image, we first formulate a 2D grid of size $\sqrt{N} \times \sqrt{N}$. For any two tokens y and w from the N tokens, their distance is defined as the Manhattan distance $d(\cdot, \cdot)$ between their positions in the 2D grid. Based on this distance metric, we construct the initial token set $E_{initial}$:

$$E_{initial} = \operatorname{argmax}_{y, w \in S} [\min (d(y, w) : \forall S \subset \mathbf{X}_I)]. \quad (11)$$

4.3 Pruning layer selection

We propose that determining which layers to prune is closely related to encoding process of image tokens. Specifically, pruning should occur either before or after the layers where the meaning of image tokens changes significantly, since it is difficult to identify truly important tokens in such layers. We compute the cosine similarity between image token hidden states X_I^l, X_I^{l+1} before and after each layer. For each layer, we plot the number of tokens with similarity below threshold τ alongside the total attention allocated to image tokens. As shown in Figure 4, it can be observed that LVLMs tends to allocate more attention to image tokens in layers following those where the representations of image tokens undergo significant changes. Based on these insights, we propose a task-independent layer selection strategy for pruning. Using a fixed set of 64 samples across all datasets, we identify layers immediately before and after major shifts in image token semantics. As shown in Figure 3, we perform pruning at selection layers, which enhances the effectiveness of our pruning strategy.

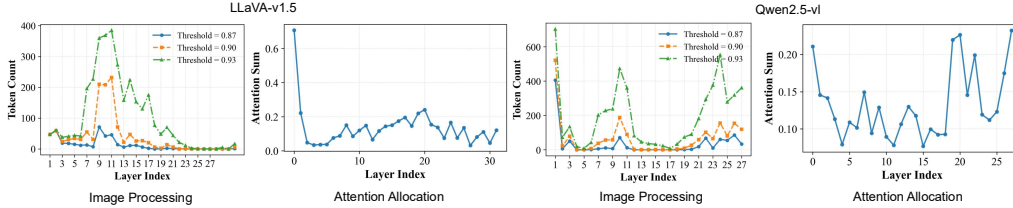


Figure 4: Layer-wise image token hidden state dynamics and attention allocation in LVLMs.

5 Experiment

Baselines and models To rigorously assess the generalizability of our proposed image token compression method, we integrate it into several state-of-the-art multimodal large models and conduct extensive experiments on diverse benchmark tasks. Specifically, we evaluate our approach on four representative models: LLaVA-v1.5-7B, LLaVA-v1.5-13B, LLaVA-v1.6-7B and Qwen2.5-VL-7B-Instruct [2, 20, 21, 22, 32]. We select several plug-and-play compression baselines that support inference-time token pruning: FastV [5] and PyramidDrop [33], which select informative tokens via attention mechanisms; DivPrune [1], which filters tokens based on visual diversity and VTW [19], which discards all image tokens at a specific transformer layer determined by validation performance.

Benchmarks and evaluation We conduct comprehensive experiments on standard visual understanding tasks using models of different sizes, model families, and compression ratios. We report the results on GQA, MMB, MME, POPE, SQA and MM-VeT [10, 15, 16, 23, 36, 37]. All experiments are carried out using the LMMs-Eval [3, 17] framework. In addition to accuracy on each dataset, we evaluate all methods in terms of FLOPs, inference latency, and KV cache memory usage. For

Table 1: Comparison of BTW with VTW, PDrop, FastV, and DivPrune across different models and datasets. *: For models using dynamic resolution, we report the token retention ratio instead of the absolute token count.

Method	Token	TFLOPS	GQA	MME	MMB _{en}	POPE	SQA	MMVET	Avg.
LLaVA-1.5-7B									
Original	576	3.82	62.0	1510.7	64.3	85.8	69.4	29.0	100%
VTW (AAAI25) [19]	236	1.67	51.3	<u>1475.0</u>	63.4	82.1	68.8	17.8	89%
PDrop (CVPR25) [33]	192	1.30	57.1	1399.0	61.6	83.6	68.4	25.8	94%
FastV (ECCV24) [5]	172	1.65	57.6	1465.0	61.6	81.0	<u>68.9</u>	29.3	96%
DivPrune (CVPR25) [1]	128	0.83	<u>58.8</u>	1405.4	62.1	<u>85.1</u>	68.4	27.4	96%
BTP(ours)	128	0.85	59.0	1487.0	<u>62.7</u>	85.6	69.1	<u>29.1</u>	98%
LLaVA-1.5-13B									
Original	576	7.44	63.2	1521.7	68.8	87.0	72.7	37.4	100%
VTW (AAAI25) [19]	236	2.97	55.6	<u>1517.1</u>	<u>67.7</u>	79.0	72.2	22.6	89%
PDrop (CVPR25) [33]	192	2.46	<u>60.5</u>	1493.0	67.3	85.1	73.7	32.8	96%
FastV (ECCV24) [5]	172	2.25	60.0	1473.0	67.0	83.6	72.9	31.9	95%
DivPrune (CVPR25) [1]	128	1.63	58.8	1461.0	65.8	<u>86.5</u>	72.6	<u>34.0</u>	96%
BTP(ours)	128	1.68	62.2	1519.7	68.0	86.9	72.7	34.5	98%
LLaVA-1.6-7B *									
Original	100%	20.82	64.2	1519.3	67.1	86.4	73.6	37.5	100%
VTW (AAAI25) [19]	40%	9.11	53.3	1472.8	65.6	84.1	68.3	16.3	85%
PDrop (CVPR25) [33]	25%	6.77	60.4	1462.6	65.1	<u>86.4</u>	<u>68.3</u>	27.4	92%
FastV (ECCV24) [5]	22%	5.76	60.3	1469.1	64.3	85.5	68.2	32.3	94%
DivPrune (CVPR25) [1]	22%	4.20	61.4	1467.9	65.4	86.2	67.4	26.9	92%
BTP(ours)	22%	4.52	<u>60.6</u>	1490.8	65.8	86.7	68.4	<u>30.3</u>	94%
Qwen2.5-VL-7B *									
Original	100%	5.48	60.4	1690.8	82.5	87.4	76.7	16.1	100%
VTW (AAAI25) [19]	40%	2.38	40.2	1129.8	58.7	61.5	69.7	4.5	65%
PDrop (CVPR25) [33]	30%	1.81	49.9	1462.5	70.6	76.8	72.6	9.58	82%
FastV (ECCV24) [5]	30%	1.79	<u>52.6</u>	1595.5	73.4	83.9	<u>74.0</u>	16.2	96%
DivPrune (CVPR25) [1]	25%	1.34	50.1	<u>1639.2</u>	76.9	<u>85.4</u>	73.0	17.5	96%
BTP(ours)	25%	1.67	57.2	1651.5	<u>75.2</u>	86.2	74.1	<u>16.8</u>	97%

inference throughout, we follow the PyramidDrop. Specifically, we calculate the FLOPs of the l -th layer’s attention and MLP modules through $4nd^2 + 2n^2d + 3ndm$. n is the number of tokens, d is the hidden state size, and m is the intermediate size of the FFN.

Implementation details All pruning experiments are conducted on 8 NVIDIA A800 GPUs using the HuggingFace Transformers library. To determine pruning stages, we randomly sample 64 instances from the LLaVA-655k [20, 21, 22] dataset and use the same set across all models and benchmarks, thus avoiding separate calibration for each benchmark. We gradually reduce the number of image tokens at each stage. In the early layers, we use a larger λ value to focus more on global information, while in the deeper layers, we use a smaller lambda to emphasize local details. More implementation details for different models are provided in the see Appendix A.2. Similar to the implementation of PyramidDrop, we compute the required attention scores separately within the **FlashAttn** module at the specified pruning layers, achieving full compatibility with **FlashAttn** [8, 9]. It is worth noting that all our experiments are conducted with **FlashAttention** acceleration enabled.

5.1 Main results

BTP outperforms SOTA methods across LVLMS As shown in Table 1, we conduct extensive experiments across different model families and parameter scales. Empirical results demonstrate that our approach consistently surpasses state-of-the-art methods on most benchmark tasks. Our method achieves **98%** of the original average performance under a **22%** compression rate across LLaVA models of different sizes. Moreover, our method consistently outperforms all models, achieving better results than both attention-based and diversity-based approaches. We also visualize the impact

of different methods on layer outputs in Figure 5, our method preserves consistency with the original outputs at both local and global levels. The Appendix A.3 further provides visualizations of the spatial distribution of image tokens selected by various methods. Our method yields more effective token selection in deeper layers.

BTP maintains stable performance across different compression ratios

We assess the performance of our method across a range of compression ratios to verify its effectiveness. We find that FLOPs account only for the computational cost of the attention and MLP modules, while ignoring the overhead introduced by additional components. As a result, FLOPs alone fail to accurately reflect the actual inference latency. Therefore, as shown in Table 2, we compare the performance and average inference time of different methods under varying compression ratios. It can be observed that although DivPrune achieves lower theoretical FLOPs, its end-to-end latency even exceeds that of the original uncompressed model. In contrast, our method leverages spatial division for initialization, significantly reducing the actual inference time. Across various compression ratios, our method consistently achieves better performance than state-of-the-art approaches on most datasets, without incurring additional computational overhead.

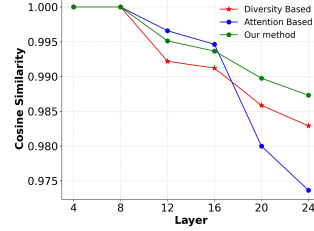


Figure 5: Effect of various pruned methods on the output of decoder layers.

Table 2: Performance comparison with FastV and DivPrune across varying compression ratios. We report the results on LLaVA-v1.5-7B.

Method	Average Token	TFLOPS	Latency	GQA	MME	MMB	SQA
LLaVA-1.5-7B	576	3.82	0.145s	62.0	1510.7	64.3	69.4
FastV	128	0.86	0.122s (15% ↓)	49.6	1388.6	56.1	60.2
DivPrune	128	0.83	0.224s (54% ↑)	58.8	1405.4	62.1	68.4
BTP(ours)	128	0.85	0.134s (7% ↓)	59.0	1487.0	62.7	69.1
FastV	64	0.42	0.118s (18% ↓)	46.1	801.3	48.0	51.1
DivPrune	64	0.41	0.150s (0.5% ↑)	57.5	1350.0	58.5	67.6
BTP(ours)	64	0.42	0.120s (17% ↓)	<u>55.0</u>	1364.1	58.6	68.3

5.2 Efficiency analysis

The additional overhead introduced by our method primarily arises from the attention computation and the selection of the diversity set. Since we compute attention only between the final token and the image tokens, the added attention complexity is $\mathcal{O}(n)$. For the selection of the diversity set, our proposed spatial initialization strategy and progressive weight decay allow us to select only a small number of additional tokens. In this section, we compare the efficiency of our method with other approaches, evaluating from multiple perspectives including theoretical FLOPs, inference latency, KV cache size, and corresponding benchmark performance. For inference latency, we report the average inference time per sample. For KV cache memory usage, we report the average GPU memory consumption after compression. We conduct experiments using LLaVA-v1.5 and LLaVA-v1.6. Notably, LLaVA-v1.6 processes images at a higher resolution, resulting in a larger number of image tokens.

Table 3: Evaluation of compression efficiency on different models

Method	Average token	Cache Size	TFLOPS	Latency	LLaVA-COCO
LLaVA-1.5-7B	576	0.34GB (100%)	3.82	2.24s	90.8
FastV	172	0.15GB (55.8% ↓)	1.65	2.11s (5% ↓)	80.6
DivPrune	128	0.11GB (67.6% ↓)	0.83	2.33s (4% ↑)	80.3
BTP(ours)	128	0.11GB (67.6% ↓)	0.85	2.13s (4% ↓)	80.9
LLaVA-1.6-7B	2880	1.11GB (100%)	20.82	4.24s	106.6
FastV	860	0.37GB (66.6% ↓)	6.45	3.77s (11% ↓)	92.6
DivPrune	633	0.28GB (74.7% ↓)	4.20	5.00s (17% ↑)	99.1
BTP(ours)	633	0.28GB (74.7% ↓)	4.52	3.91s (7% ↓)	98.9

As shown in Table 3, our method achieves the best performance while maintaining practical efficiency.

5.3 Ablation study

Choice of balance factor value: We first analyze the effect of λ in the local-global objective functions. This factor determines the trade-off at each layer between preserving local outputs and contributing to the global output. We gradually increase the value of λ . We define the ratio between the performance of the pruned model and that of the base model on the target task as the performance gain. The computation of performance gain is detailed in the Appendix A.4. As shown in Figure 6, we conduct experiments on both LLaVA-v1.5 and LLaVA-v1.6 to evaluate the effectiveness of our approach. As illustrated, model performance peaks when λ balances the two objectives. In contrast, relying solely on either the local or global objective leads to a decline in performance. This highlights the importance of our method in effectively balancing the two objectives. Therefore, we use smaller λ values (0.5–0.7) in the shallow layers and larger values (0.8–1.0) in the deeper layers.

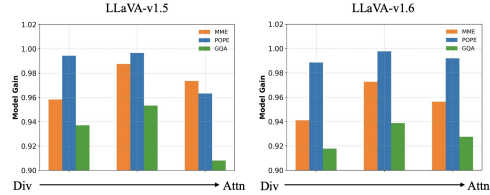


Figure 6: Ablation study on balance factor.

Effectiveness of rebalanced attention and spatial diversity initialization: We then perform ablation studies on the attention rebalance module and the spatial initialization module. We experimented with various combinations of the two modules. The results are presented in Table 4. It can be observed that removing the attention rebalance module results in a significant degradation in model performance. This degradation arises from the inherent bias in attention mechanisms, where positional encodings tend to shift attention disproportionately toward later tokens, leading to suboptimal token selection. On the other hand, omitting the spatial initialization module causes a marked increase in inference latency, in some cases even surpassing that of the original unpruned model. This suggests that while pruning reduces token count, naive initialization can introduce computational overhead that negates the benefits of pruning, thereby limiting the method’s applicability in latency-sensitive real-world scenarios. This demonstrates the effectiveness of the proposed module in improving both model performance and inference speed.

Table 4: Ablation study on attention rebalance module and spatial initialization module.

RA	SI	Latency	MME	GQA	POPE
✓	✓	0.134s	1487.0	59.0	85.6
✓		0.232s	1486.5	57.9	86.4
	✓	0.140s	1464.6	57.4	85.1
		0.131s	1478.1	57.3	84.4

Effectiveness of calibration-based pruning stage selection: To evaluate the effectiveness of our proposed calibration-based pruning stage selection, we compare it with a baseline that uniformly divides the pruning stages according to the total number of decoder layers, under the same compression rate. Experimental results are shown in Table 5. We observe that our pruning layer selection method outperforms uniform selection. This is especially evident on Qwen2.5-VL, where uniform selection leads to a significant performance drop. We attribute this to differences in how Qwen2.5-VL processes image tokens as shown in Figure 4.

Table 5: Ablation study on layer selection strategy.

Method	Stage Selection	MME	MMB
LLaVa-v1.5	Averaged	1483.2	62.3
	Ours	1487.0	62.7
LLaVa-v1.6	Averaged	1480.1	64.7
	Ours	1490.8	65.8
Qwen2.5-vl	Averaged	1551.6	73.8
	Ours	1641.5	75.2

6 Conclusion

In this work, we conduct initial studies to investigate and verify the limitations of existing image token pruning methods. We further analyze the impact of two pruning strategies on model performance from the perspective of the objective function, and formulate a local-global pruning optimization objective. To reduce information loss during pruning, we propose **Balanced Token Pruning (BTP)**, a multi-stage pruning method. We first determine the pruning stages using a calibration set. In the early layers, we focus on a *diversity-oriented objective* to account for the influence of pruning on deeper layers, while in the later layers, we adopt an *attention-based objective* to better preserve local

information. Experiments on several popular models and multiple visual understanding benchmarks demonstrate the effectiveness of our approach. We hope our method can inspire further research on visual token redundancy and the design of more efficient multimodal large models.

References

- [1] Saeed Ranjbar Alvar, Gursimran Singh, Mohammad Akbari, and Yong Zhang. Divprune: Diversity-based visual token pruning for large multimodal models. *arXiv preprint arXiv:2503.02175*, 2025.
- [2] Shuai Bai, Keqin Chen, Xuejing Liu, Jialin Wang, Wenbin Ge, Sibor Song, Kai Dang, Peng Wang, Shijie Wang, Jun Tang, et al. Qwen2.5-vl technical report. *arXiv preprint arXiv:2502.13923*, 2025.
- [3] Li* Bo, Zhang* Peiyuan, Zhang* Kaichen, Pu* Fanyi, Du Xinrun, Dong Yuhao, Liu Haotian, Zhang Yuanhan, Zhang Ge, Li Chunyuan, and Ziwei Liu. Lmms-eval: Accelerating the development of large multimodal models, March 2024.
- [4] Jieneng Chen, Luoxin Ye, Ju He, Zhao-Yang Wang, Daniel Khashabi, and Alan Yuille. Efficient large multi-modal models via visual context compression. In *The Thirty-eighth Annual Conference on Neural Information Processing Systems*, 2024.
- [5] Liang Chen, Haozhe Zhao, Tianyu Liu, Shuai Bai, Junyang Lin, Chang Zhou, and Baobao Chang. An image is worth 1/2 tokens after layer 2: Plug-and-play inference acceleration for large vision-language models. In *European Conference on Computer Vision*, pages 19–35. Springer, 2024.
- [6] Zhe Chen, Jiannan Wu, Wenhai Wang, Weijie Su, Guo Chen, Sen Xing, Muyan Zhong, Qinglong Zhang, Xizhou Zhu, Lewei Lu, et al. Internvl: Scaling up vision foundation models and aligning for generic visual-linguistic tasks. In *Proceedings of the IEEE/CVF Conference on Computer Vision and Pattern Recognition*, pages 24185–24198, 2024.
- [7] Moulik Chauraria, Xinbo Wu, Sourya Basu, Nitesh Sekhar, Yue Wu, Xu Zhang, Prateek Singhal, and Lav R. Varshney. Semantically grounded qformer for efficient vision language understanding, 2024.
- [8] Tri Dao. FlashAttention-2: Faster attention with better parallelism and work partitioning. In *International Conference on Learning Representations (ICLR)*, 2024.
- [9] Tri Dao, Daniel Y. Fu, Stefano Ermon, Atri Rudra, and Christopher Ré. FlashAttention: Fast and memory-efficient exact attention with IO-awareness. In *Advances in Neural Information Processing Systems (NeurIPS)*, 2022.
- [10] Chaoyou Fu, Peixian Chen, Yunhang Shen, Yulei Qin, Mengdan Zhang, Xu Lin, Jinrui Yang, Xiawu Zheng, Ke Li, Xing Sun, et al. Mme: A comprehensive evaluation benchmark for multimodal large language models. *arXiv preprint arXiv:2306.13394*, 2023.
- [11] Zhangwei Gao, Zhe Chen, Erfei Cui, Yiming Ren, Weiyun Wang, Jinguo Zhu, Hao Tian, Shenglong Ye, Junjun He, Xizhou Zhu, et al. Mini-internvl: a flexible-transfer pocket multimodal model with 5% parameters and 90% performance. *Visual Intelligence*, 2(1):1–17, 2024.
- [12] Wenxuan Huang, Zijie Zhai, Yunhang Shen, Shaosheng Cao, Fei Zhao, Xiangfeng Xu, Zheyu Ye, Yao Hu, and Shaohui Lin. Dynamic-llava: Efficient multimodal large language models via dynamic vision-language context sparsification. *arXiv preprint arXiv:2412.00876*, 2024.
- [13] Wenxuan Huang, Zijie Zhai, Yunhang Shen, Shaosheng Cao, Fei Zhao, Xiangfeng Xu, Zheyu Ye, Yao Hu, and Shaohui Lin. Dynamic-llava: Efficient multimodal large language models via dynamic vision-language context sparsification, 2025.
- [14] Itay Hubara, Yury Nahshan, Yair Hanani, Ron Banner, and Daniel Soudry. Accurate post training quantization with small calibration sets. In *International Conference on Machine Learning*, pages 4466–4475. PMLR, 2021.

- [15] Drew A Hudson and Christopher D Manning. Gqa: A new dataset for real-world visual reasoning and compositional question answering. In *Proceedings of the IEEE/CVF conference on computer vision and pattern recognition*, pages 6700–6709, 2019.
- [16] Mohit Iyyer, Wen-tau Yih, and Ming-Wei Chang. Search-based neural structured learning for sequential question answering. In *Proceedings of the 55th Annual Meeting of the Association for Computational Linguistics (Volume 1: Long Papers)*, pages 1821–1831, 2017.
- [17] Zhang Kaichen, Li Bo, Zhang Peiyuan, Pu Fanyi, Cahyono Joshua-Adrian, Hu Kairui, Liu Shuai, Zhang Yuanhan, Yang Jingkan, Li Chunyuan, and Liu Ziwei. Lmms-eval: Reality check on the evaluation of large multimodal models, 2024.
- [18] Junnan Li, Dongxu Li, Caiming Xiong, and Steven Hoi. Blip: Bootstrapping language-image pre-training for unified vision-language understanding and generation, 2022.
- [19] Zhihang Lin, Mingbao Lin, Luxi Lin, and Rongrong Ji. Boosting multimodal large language models with visual tokens withdrawal for rapid inference. In *Proceedings of the AAAI Conference on Artificial Intelligence*, volume 39, pages 5334–5342, 2025.
- [20] Haotian Liu, Chunyuan Li, Yuheng Li, and Yong Jae Lee. Improved baselines with visual instruction tuning, 2023.
- [21] Haotian Liu, Chunyuan Li, Yuheng Li, Bo Li, Yuanhan Zhang, Sheng Shen, and Yong Jae Lee. Llava-next: Improved reasoning, ocr, and world knowledge, January 2024.
- [22] Haotian Liu, Chunyuan Li, Qingyang Wu, and Yong Jae Lee. Visual instruction tuning, 2023.
- [23] Yuan Liu, Haodong Duan, Yuanhan Zhang, Bo Li, Songyang Zhang, Wangbo Zhao, Yike Yuan, Jiaqi Wang, Conghui He, Ziwei Liu, et al. Mmbench: Is your multi-modal model an all-around player? In *European conference on computer vision*, pages 216–233. Springer, 2024.
- [24] Zirui Liu, Jiayi Yuan, Hongye Jin, Shaochen Zhong, Zhaozhuo Xu, Vladimir Braverman, Beidi Chen, and Xia Hu. Kivi: A tuning-free asymmetric 2bit quantization for kv cache. *arXiv preprint arXiv:2402.02750*, 2024.
- [25] Daniel Cosmin Porumbel, Jin-Kao Hao, and Fred Glover. A simple and effective algorithm for the maxmin diversity problem. *Annals of Operations Research*, 186:275–293, 2011.
- [26] Alec Radford, Jong Wook Kim, Chris Hallacy, Aditya Ramesh, Gabriel Goh, Sandhini Agarwal, Girish Sastry, Amanda Askell, Pamela Mishkin, Jack Clark, Gretchen Krueger, and Ilya Sutskever. Learning transferable visual models from natural language supervision, 2021.
- [27] Charles C Ragin. Fuzzy sets: Calibration versus measurement. *Methodology volume of Oxford handbooks of political science*, 2, 2007.
- [28] Mauricio GC Resende, Rafael Martí, Micael Gallego, and Abraham Duarte. Grasp and path relinking for the max–min diversity problem. *Computers & Operations Research*, 37(3):498–508, 2010.
- [29] Yuzhang Shang, Mu Cai, Bingxin Xu, Yong Jae Lee, and Yan Yan. Llava-prumerge: Adaptive token reduction for efficient large multimodal models. *arXiv preprint arXiv:2403.15388*, 2024.
- [30] Hugo Touvron, Thibaut Lavril, Gautier Izacard, Xavier Martinet, Marie-Anne Lachaux, Timothée Lacroix, Baptiste Rozière, Naman Goyal, Eric Hambro, Faisal Azhar, Aurelien Rodriguez, Armand Joulin, Edouard Grave, and Guillaume Lample. Llama: Open and efficient foundation language models. *arXiv preprint arXiv:2302.13971*, 2023.
- [31] Ashish Vaswani, Noam Shazeer, Niki Parmar, Jakob Uszkoreit, Llion Jones, Aidan N Gomez, Łukasz Kaiser, and Illia Polosukhin. Attention is all you need. *Advances in neural information processing systems*, 30, 2017.
- [32] Peng Wang, Shuai Bai, Sinan Tan, Shijie Wang, Zhihao Fan, Jinze Bai, Keqin Chen, Xuejing Liu, Jialin Wang, Wenbin Ge, et al. Qwen2-vl: Enhancing vision-language model’s perception of the world at any resolution. *arXiv preprint arXiv:2409.12191*, 2024.

- [33] Long Xing, Qidong Huang, Xiaoyi Dong, Jiajie Lu, Pan Zhang, Yuhang Zang, Yuhang Cao, Conghui He, Jiaqi Wang, Feng Wu, et al. Pyramiddrop: Accelerating your large vision-language models via pyramid visual redundancy reduction. *arXiv preprint arXiv:2410.17247*, 2024.
- [34] Senqiao Yang, Yukang Chen, Zhuotao Tian, Chengyao Wang, Jingyao Li, Bei Yu, and Jiaya Jia. Visionzip: Longer is better but not necessary in vision language models. *arXiv preprint arXiv:2412.04467*, 2024.
- [35] Xubing Ye, Yukang Gan, Yixiao Ge, Xiao-Ping Zhang, and Yansong Tang. Atp-llava: Adaptive token pruning for large vision language models. *arXiv preprint arXiv:2412.00447*, 2024.
- [36] Li Yifan, Du Yifan, Zhou Kun, Wang Jinpeng, Zhao Wayne-Xin, and Ji-Rong Wen. Evaluating object hallucination in large vision-language models. In *The 2023 Conference on Empirical Methods in Natural Language Processing*, 2023.
- [37] Weihao Yu, Zhengyuan Yang, Linjie Li, Jianfeng Wang, Kevin Lin, Zicheng Liu, Xinchao Wang, and Lijuan Wang. Mm-vet: Evaluating large multimodal models for integrated capabilities. In *International conference on machine learning*. PMLR, 2024.
- [38] Shaolei Zhang, Qingkai Fang, Zhe Yang, and Yang Feng. Llava-mini: Efficient image and video large multimodal models with one vision token. *arXiv preprint arXiv:2501.03895*, 2025.
- [39] Shaolei Zhang, Qingkai Fang, Zhe Yang, and Yang Feng. Llava-mini: Efficient image and video large multimodal models with one vision token, 2025.
- [40] Lianmin Zheng, Wei-Lin Chiang, Ying Sheng, Siyuan Zhuang, Zhanghao Wu, Yonghao Zhuang, Zi Lin, Zhuohan Li, Dacheng Li, Eric. P Xing, Hao Zhang, Joseph E. Gonzalez, and Ion Stoica. Judging llm-as-a-judge with mt-bench and chatbot arena, 2023.

A Appendix

A.1 Key and Value of LVLMs

Following previous works on token quantization KIVI [24], we visualize the K_l and V_l of different LVLMs, the results are shown below:

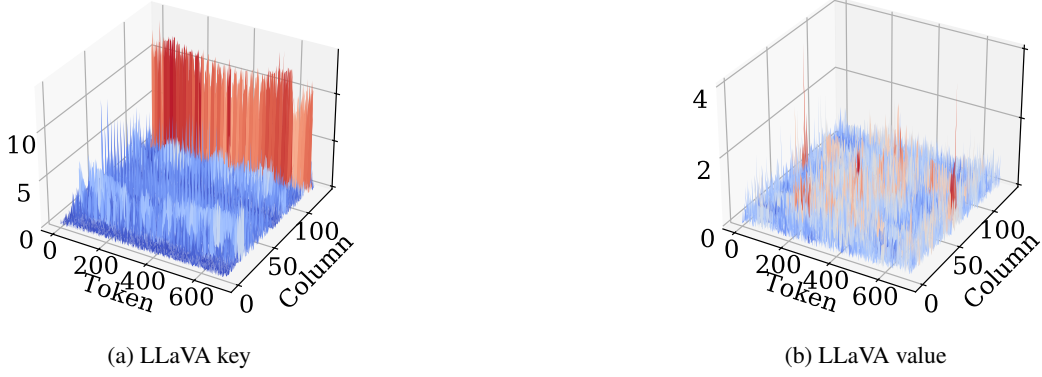


Figure 7: Visualization of key and value of LLaVA-v1.5

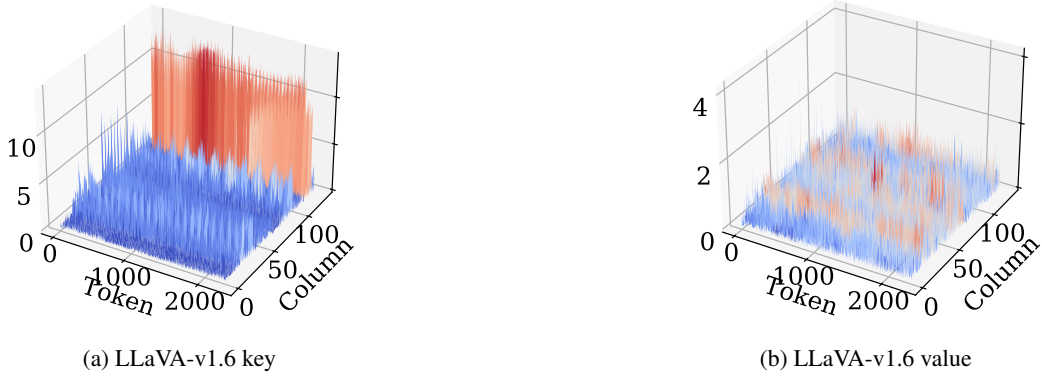


Figure 8: Visualization of key and value of LLaVA-v1.6



Figure 9: Visualization of key and value of Qwen2.5-vl

A.2 Experiment Settings

For LLaVA-v1.5-7B, LLaVA-v1.5-13B, and LLaVA-v1.6-7B, we divide the pruning process into five stages based on the image token handling pipeline described in the Appendix. In each stage, except for the last one, we retain 50% of the tokens from the previous stage. In the final stage, all tokens are discarded to maximize inference speed. For Qwen2.5-VL, since its image token processing can be clearly divided into two stages, we retain 25% of the tokens in the fourth stage and 12.5% in the final stage to preserve model performance.

A.3 Visualization of token selection under different pruning strategies

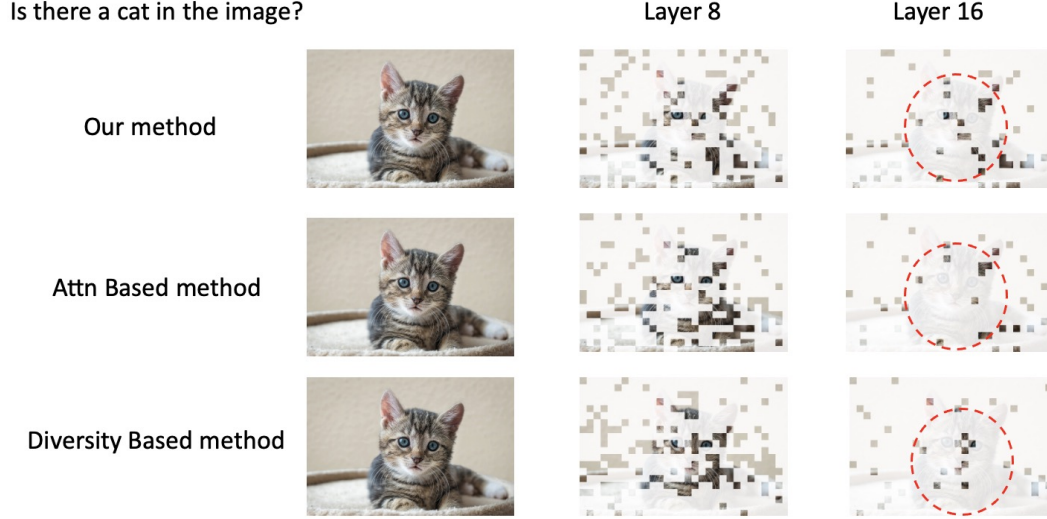


Figure 10: Visualization of Image Token Selection Across Different Methods

A.4 Calculation of model gain

Since evaluation metrics vary across tasks and the difficulty levels differ significantly, it is not reasonable to present all task results directly in a unified format. For example, the original LLaVA-v1.5 model scores 1510 on the MME benchmark but only 62 on GQA. To address this, we define a model gain metric as:

$$Gain = \text{Normalize}\left(\frac{Pruned_{score}}{Original_{score}}\right). \quad (12)$$